

Does the Amati Correlation Exhibit Redshift-Driven Heterogeneity in Long GRBs?

Darshan Singh^{a,b}, Meghendra Singh^c, Dinkar Verma^a, Kanhaiya Lal Pandey^d,
Shashikant Gupta^{a,*}

^a*Department of Basic and Applied Sciences, GD Goenka
University, Gurugram, 122103, Haryana, India*

^b*Department of Physics, Mata Raj Kaur Institute of Engineering and
Technology, Rewari, 123401, Haryana, India*

^c*Delhi Metro Rail Corporation Limited, New Delhi, 110001, Delhi, India*

^d*Department of Physics, School of Advanced Sciences, Vellore Institute of
Technology, Vellore, 632014, Tamil Nadu, India*

Abstract

Long gamma-ray bursts (GRBs) offer significant insights into cosmology due to their high energy emissions and the potential to probe the early universe. The Amati relation, which links the intrinsic peak energy to the isotropic energy, is crucial for understanding their cosmological applications. This study investigates the redshift-driven heterogeneity of the Amati correlation in long GRBs. We analyzed 221 long GRBs with redshifts from 0.034 to 8.2, dividing them by redshift thresholds of 1.5 and 2. Using Bayesian marginalization and Reichart's likelihood approach, we found significant differences in the Amati parameters between low and high redshift subgroups. These variations, differing by approximately 2σ at $z = 1.5$ and more than 1σ at $z = 2$, suggest an evolution in the GRB population with redshift, possibly reflecting changes in host galaxy properties. However, selection effects and instrumental biases may also contribute to it. Our results challenge the assumption of the Amati relation's universality and underscore the need for larger datasets and more precise measurements from upcoming missions like Transient High-Energy Sky and Early Universe Surveyor (THESEUS), and enhanced X-ray Timing and Polarimetry mission (eXTP) to refine our understanding of GRB physics.

Keywords: Cosmology, Gamma ray burst, Large-scale structure of the universe,

*Corresponding author

1. Introduction

Gamma-ray bursts (GRBs), observed as intense flashes of gamma rays in distant galaxies, represent some of the most energetic explosions in the universe [1, 2]. A key characteristic of GRBs is their pulse duration, commonly quantified by the parameter T_{90} [3], defined as the time interval during which 90% of the total background-subtracted gamma-ray photons are detected. Based on T_{90} , GRBs are classified into two main types: short GRBs, lasting less than 2 seconds and typically resulting from the merger of compact objects like neutron stars or black holes; and long GRBs, lasting more than 2 seconds and believed to be associated with the collapse of massive stars into black holes [2, 4]. Long GRBs are particularly valuable for cosmological studies due to their longer pulse duration, facilitating localization within their host galaxies and redshift measurement. They can help measure cosmological distances, probe the early universe, and provide constraints on cosmic reionization and star formation rates. Correlations among various GRB observables are important to calibrate the observational data for distance measurement. Among the various correlations observed, the Amati relation [5, 6, 7, 8], which links the intrinsic peak energy ($E_{p,i}$) to its equivalent isotropic energy (E_{iso}), has been a subject of particular interest. $E_{p,i}$ is computed from the observed peak energy E_{peak} in the νF_ν spectrum of a burst as $E_{p,i} = E_{peak}(1+z)$. Originally expressed in exponential form, the Amati relation is now commonly presented in linear form for its elegance:

$$\log E_{iso} = a + b \log E_{p,i}, \quad (1)$$

where the intercept, a and the slope, b are known as Amati parameters. The parameter b is usually positive indicating a positive correlation between E_{iso} and $E_{p,i}$ while a is negative. Alongside the Yonetoku relation between E_{peak} and the isotropic peak luminosity, L_{iso} [9]; Ghirlanda relation between E_{peak} and collimation-corrected energy, E_γ [10, 11]; and Dianotti relation [12]; Amati relation serves as a cornerstone for probing the physics of GRBs and their use as cosmological tools [13, 14, 15, 16]. Several studies have attempted to constrain cosmological parameters using GRB data [17, 18, 19, 20, 21, 22]. However, a critical question arises regarding whether the relations used for cosmological applications remain constant throughout the history of the universe or evolve with redshift, a measure of the cosmic scale and the age of the universe at the time of

the burst [23]. GRBs are calibrated using type Ia supernovae for cosmological applications, which can be observed only up to $z = 1.75$. If high-redshift GRBs differ from their low-redshift counterparts, their calibration may be questionable. Recent studies have presented conflicting views on the evolution of the Amati parameters with redshift. Some research suggests that the Amati parameters, a and b , may systematically vary with the mean redshift of GRBs. By dividing a sample of long-duration GRBs into redshift-based groups and fitting the Amati relation separately to each group, significant and systematic changes in the parameters with redshift have been observed [15, 16, 21, 24, 25, 26, 27, 28]. Monte Carlo simulations further support that this variation is unlikely due to selection effects from the fluence limit, indicating a strong evolution of GRBs with cosmological redshift [24]. In a recent study [29], it is concluded that the Amati relation of GRBs evolves with z . Conversely, other studies [30, 31] challenge this view by using different samples of GRBs and investigating the redshift independence of the Amati and Yonetoku relations. By binning the data by redshift and fitting both relations, these studies found that the normalization and slope do not exhibit systematic evolution with redshift, implying that the Amati and Yonetoku relations are redshift-independent. The discrepancy between these findings raises important questions about the intrinsic properties of GRBs and their use as standard candles in cosmology.

Differences in the properties of GRBs at different redshifts, if exist, may reflect signatures of cosmic evolution. For instance, the peak of star formation in cosmic history at $z = 1.5 - 2$ could be detected in GRB properties. Substantial evidence indicates evolutionary shifts in the demographics of various galaxy morphologies with increasing redshift. Notably, there is a significant decline in the proportion of disk galaxies around $z = 2$ [32] accompanied by a corresponding increase in peculiar types. However, for massive galaxies, the fractions of disks, spheroids, and peculiar types appear to remain relatively constant within the redshift range of $1.5 < z < 6.5$. Furthermore, galaxy morphologies exhibit limited correlation with other key physical properties such as star formation rate, color, mass, or size [33, 34, 35]. Mass distribution of host galaxies and the redshift distribution of long GRBs, as investigated by [36] indicates that GRB host galaxies are metallicity biased tracers of star formation. At high redshift, the early-type galaxies can be observed in the active star formation period, during which massive star explosions and galactic winds occur. This situation is not found at lower redshift, where star formation is already quenched for this morphological type [37] which might be linked to a low GRB rate. Contrary to this, recent observations by the James Webb Space Telescope (JWST) have identified massive galaxies at high redshifts, posing

a challenge to the standard Λ CDM cosmological model [38].

To address this knowledge gap, i.e., whether there are two different populations of long GRBs at low and high redshifts, this study investigates the differences in Amati parameters in the low and high- z regimes. In Section 2, we will describe our methodology, including the data and the analysis techniques employed. Section 3 presents the key findings of our research and discusses the implications of these findings. Finally, Section 4 will conclude the paper by summarizing the main points and suggesting avenues for future research.

2. Data and Methodology

2.1. GRB Data Sample

Investigating the evolution of GRBs with redshift requires large datasets of long GRBs covering a wide range of redshifts. In a previous study, [28] used 162 long GRBs compiled by [18] to explore differences between low and high-redshift GRB populations. However, [39] and [20] have raised concerns about the suitability of this dataset for cosmological applications, noting that the constraints derived from these GRBs show inconsistencies with those obtained from other cosmological probes such as Type Ia supernovae, BAO, $H(z)$ measurements, and CMB anisotropy data. To address these concerns and validate the results of [28], a larger dataset with more accurate measurements of GRB observables is required. In the current study, we utilize a more comprehensive and recent dataset compiled by [21], containing 221 long GRBs spanning a redshift range of $0.034 \leq z \leq 8.2$. While many GRBs in this new dataset overlap with the previous 162-GRB sample, they benefit from updated values of key parameters, including isotropic equivalent energy and peak energy. This dataset primarily derives from the joint observations conducted by Swift and Fermi satellites.

In some cases, $E_{p,i}$ is provided directly by Swift which has significantly contributed to detecting several GRBs with their redshifts. Swift is equipped with three instruments: the Burst Alert Telescope (BAT) for GRB detection, the X-ray Telescope (XRT), and the Ultra-Violet and Optical Telescope (UVOT). BAT, with its large field of view, detects GRBs in the energy range of 15 keV to 150 keV. Upon detection, the satellite slews to the burst direction for XRT and UVOT observations. The energy range of XRT is 0.2-10 keV, while the UVOT is capable of observations in the 170 – 600 nm wavelength range [40]. The Fermi Gamma-Ray Space Telescope (FGST), launched by NASA in 2008, has become a cornerstone in the study of high-energy gamma rays [41]. The primary instrument onboard FGST is the Large Area Telescope (LAT), a high-energy gamma-

Table 1: Description of GRB data (G) and its subgroups. Groups G_1 and G_2 belong to the division at $z = 1.5$, while G'_1 and G'_2 belong to the division at $z = 2$.

Group(s)	Number of GRBs	z_{min}	z_{max}	Median z
G	221	0.034	8.20	1.619
G_1	100	0.034	1.489	0.893
G_2	121	1.517	8.20	2.452
G'_1	132	0.034	1.98	1.10
G'_2	89	2.006	8.20	2.77

ray imaging telescope with a wide field of view, operating in the energy range from below 20 MeV to more than 300 GeV. Additionally, Fermi is equipped with the Gamma-ray Burst Monitor (GBM) and the Anticoincidence Detector (ACD), which complement the observations made by the LAT. The LAT provides unprecedented sensitivity across a broad energy range, spanning approximately 20 MeV to 300 GeV, making Fermi an invaluable tool in high-energy astrophysics.

2.2. Methodology

Below we discuss the technique used for our analysis, A part of it has been presented in [28].

2.2.1. Computing best-fit of Amati Parameters

The observed values of the peak energy ($E_{p,i}$) and isotropic-equivalent energy (E_{iso}) along with their uncertainties, are available for all the GRBs in the data set. For the linear form of the Amati relation, i.e, Eq. 1 among the logarithm of the observational quantities, we define χ^2 as:

$$\chi^2 = \sum_{i=1}^N \left(\frac{g^i - f(E_{p,i}^i; a, b)}{\sigma^i} \right)^2, \quad (2)$$

where $g^i = \log E_{iso}^i$, is obtained from data, and f is the value of $\log E_{iso}$ derived using Amati relation, i.e., corresponding to given $E_{p,i}^i$ (see Eq. 1). The uncertainty σ_i in $\log E_{iso}^i$ can be calculated as described in [28]:

$$\sigma_i^2 = (dE_{iso}/E_{iso})^2 + b^2(dE_{p,i}/E_{p,i})^2. \quad (3)$$

The likelihood, $P(D|M)$, which represents the probability of obtaining the data for the given model M can be expressed as:

$$P(D|M(a, b)) \propto e^{-\chi^2/2}, \quad (4)$$

where χ^2 is defined by Eq. 2. The best-fit values of the Amati parameters (a and b) can be estimated by minimizing χ^2 in Eq. 2 or by maximizing likelihood in Eq. 4. However, this method does not provide direct probabilities of these parameters, thus we employ the Bayesian approach. The direct probability of the model M , also known as the posterior probability can be easily calculated using Bayes' theorem :

$$P(M(a, b)|D) \propto P(D|M(a, b))P(M(a, b)). \quad (5)$$

Here, $P(M(a, b))$ represents the prior probability of the model. One should be cautious while selecting the prior probability as it can include personal biases and lead to an inappropriate posterior probability distribution. An advantage of the Bayesian approach is the ability to marginalize the undesired parameters. For example, marginalization on parameter b can be performed by integrating over it:

$$P(a|I) = \int P(I|a, b)P(a, b)db. \quad (6)$$

To determine whether the Amati parameters systematically increase or decrease with redshift, we fit the Amati relation in Eq. 1 for each subgroup of data using the aforementioned methods.

2.2.2. Intrinsic Scatter In the Amati relation

The correlation between E_p and E_{iso} exhibits variability often attributed to inherent scatter [28, 42]. To mitigate this variability, we employ Reichart's likelihood function, which incorporates the intrinsic scatter (σ_{int}) along with the linear relation described by Eq. 1 and is given as

$$L_{Reichart}(a, b, \sigma_{int}) = \frac{1}{2} \frac{\sum \log(\sigma_{int}^2 + \sigma_{y_i}^2 + a^2\sigma_{x_i}^2)}{\log(1 + a^2)} + \frac{1}{2} \sum \frac{(y_i - ax_i - b)^2}{\sigma_{int}^2 + \sigma_{y_i}^2 + a^2\sigma_{x_i}^2}. \quad (7)$$

The correlation function, $L_{Reichart}(a, b, \sigma_{int})$, now involves three parameters. These parameters can be simultaneously fitted, or the parameter b can be analyti-

cally evaluated by setting $\frac{\partial}{\partial b}L(a, b, \sigma_{int}) = 0$. This yields:

$$b = \left[\sum \frac{y_i - ax_i}{\sigma_{int}^2 + \sigma_{y_i}^2 + a^2\sigma_{x_i}^2} \right] \left[\sum \frac{1}{\sigma_{int}^2 + \sigma_{y_i}^2 + a^2\sigma_{x_i}^2} \right]^{-1}. \quad (8)$$

To comprehend the impact of intrinsic scatter, we concurrently determine the optimal values for parameters a , b , and σ_{int} using the aforementioned three-parameter likelihood function defined by Eq. 7. During the computation of the optimal value for one of the parameters, Bayesian marginalization is applied to the remaining two parameters. The same approach is applied to the different subgroups of the data as well.

2.2.3. Separate Fits to Low and High- z GRBs

As discussed in Section 1, galaxy populations exhibit significant differences in metallicity below and above a critical redshift, ranging from approximately 1.5 to 2. The GRB production rate depends on the metallicity of the host galaxy [43]. To explore the potential differences between GRBs below and above the critical redshift, we aim to examine the variations in the Amati parameters with redshift. For this purpose, we divide the data sample (hereafter G), containing 221 GRBs, into subgroups of low and high redshift. When the critical redshift is set at $z = 1.5$, the low- z sample consists of 100 GRBs, with a median redshift of 0.893 and a redshift range of $0.034 < z < 1.489$. The high- z sample comprises 121 GRBs, within a redshift range of $1.517 < z < 8.2$ and a median redshift of 2.452. These subgroups are referred to as G_1 and G_2 , respectively. When the critical redshift is set at $z = 2$, the low- z sample includes 132 GRBs, with a median redshift of 1.10 and a redshift range of $0.034 < z < 1.98$. The high- z sample consists of 89 GRBs, within a redshift range of $2.006 < z < 8.2$ and a median redshift of 2.77. These subgroups are referred to as G'_1 and G'_2 , respectively.

GRB observations indicate a statistically isotropic distribution of their positions [44, 45]. A large number of GRBs is required to further investigate any potential deviations from isotropy [46]. To avoid any directional biases, we aim to ensure that our GRB sample and its subgroups adequately cover the sky. The positions of the 221 GRBs in our sample are plotted in Fig. 1, demonstrating fair sky coverage. Additionally, we plot the positions of low and high- z GRBs separately in Fig. 2. Both subgroups exhibit fair sky coverage, indicating no clustering of GRBs in any particular region of the sky.

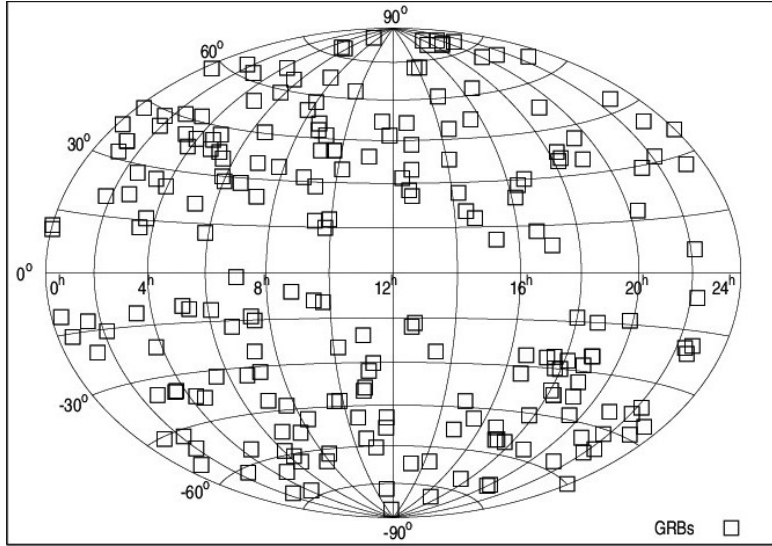


Figure 1: This celestial map shows the isotropic distribution of 221 gamma-ray bursts (GRBs) across the sky.

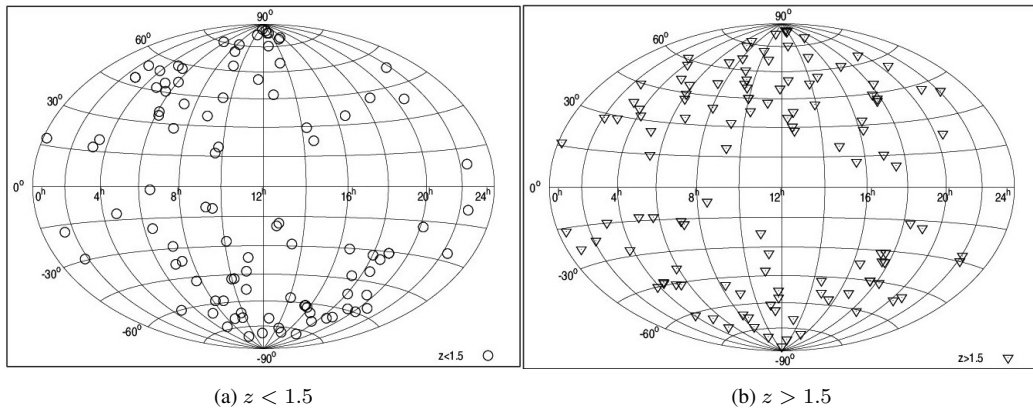


Figure 2: This celestial map shows the isotropic distribution of low and high- z gamma-ray bursts (GRBs) across the sky to ensure the fair sky coverage of the subgroups.

2.2.4. Model Selection using Akaike Information Criterion

In this study, we employed two approaches to obtain the best-fit values of the Amati parameters: (1) a single linear regression applied over the entire redshift range, and (2) separate linear regressions for different redshift ranges. To compare the performance of these approaches, we utilized the Akaike Information Criterion (AIC) [47, 48], a widely used tool for model selection. For the single linear regression across the full redshift range, the AIC is defined as

$$AIC_{Full} = 2k - 2\log(L_{full}), \quad (9)$$

where k represents the number of model parameters, and L_{full} is the maximum likelihood of the linear model for the complete dataset. It is important to note that in the chi-squared statistic, χ^2 , introduced in Eq. 2, is additive. The likelihood function L is proportional to $\exp(-\chi^2/2)$, and for independent observations, the total likelihood is obtained by multiplying the individual likelihoods. Accordingly, to compute the AIC for the subgroup analysis, we multiply the likelihoods for each redshift group, assuming the independence of observations for individual GRBs. The AIC for the grouped analysis is given by

$$AIC_{Groups} = 2k - 2\log(L_{low-z} \times L_{high-z}), \quad (10)$$

where L_{low-z} and L_{high-z} are the likelihoods of the linear models for the low-redshift and high-redshift subgroups, respectively. Lower AIC values indicate a better-fitting model by penalizing models with excessive complexity, thereby reducing the risk of overfitting. To quantify the difference between the models, we define ΔAIC as

$$\Delta AIC = AIC_{Full} - AIC_{Groups}. \quad (11)$$

The ΔAIC value helps determine whether the compared models differ significantly in terms of their fit to the data. If $\Delta AIC \geq 2$, the difference is considered significant, with the model having the lower AIC value being preferred.

3. Results and Discussion

In this section, we present our main results and highlight the possible instrumental biases that could be responsible for any differences between the low and high- z GRB properties. Toward the end of the present section, we also discuss the main differences in the properties of host galaxies of low and high- z long GRBs.

Table 2: Best-fit values of Amati parameters (a , b and σ_{int}) along with their 1σ errors for data sample G (221 GRBs) and its subgroups G_1 and G_2 . The cut-off has been taken at $z = 1.5$ to divide the data into subgroups. The Bayesian marginalization has been employed to determine the best-fit value of each parameter.

Data Set	a	b	σ_{int}
G	-6.30 ± 0.40	1.46 ± 0.07	0.93 ± 0.05
$G_1(100)$	-7.05 ± 0.55	1.56 ± 0.09	0.95 ± 0.08
$G_2(121)$	-4.20 ± 0.70	1.14 ± 0.12	0.88 ± 0.07

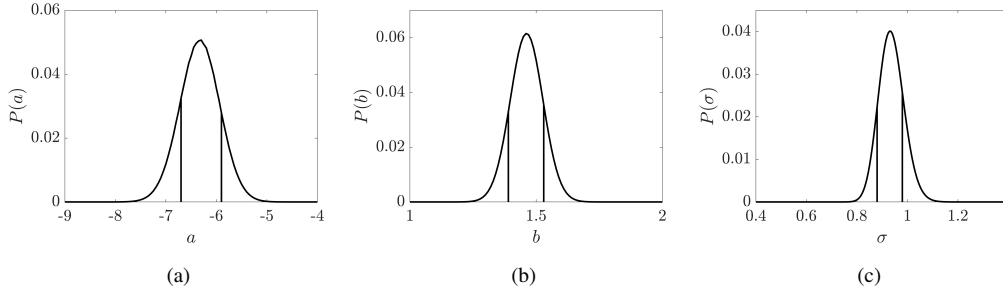


Figure 3: Distribution of posterior probability for Amati parameters a , b and σ_{int} for data sample G (221GRBs).

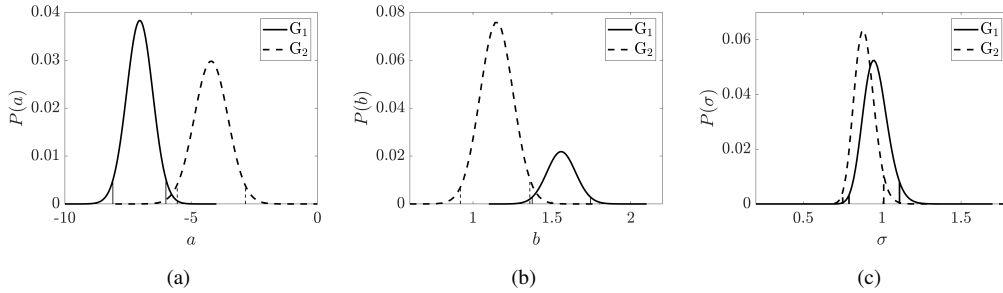


Figure 4: Posterior probability distributions of Amati parameters a , b and σ_{int} for low- z GRBs (group G_1) and high- z GRBs (group G_2) with the threshold at $z = 1.5$. The low- z and high- z distributions are not in agreement and their difference is statistically significant at more than 2σ confidence level for parameters a and b .

Table 3: Best-fit values of a , b and σ_{int} along with their 1σ errors for the subgroups G'_1 and G'_2 . The cut-off has been taken at $z = 2$ to divide the data into subgroups. The Bayesian marginalization has been employed to determine the best-fit value of each parameter.

Data Set	a	b	σ_{int}
G'_1	-6.75 ± 0.50	1.52 ± 0.09	0.99 ± 0.07
G'_2	-4.60 ± 0.75	1.21 ± 0.12	0.80 ± 0.07

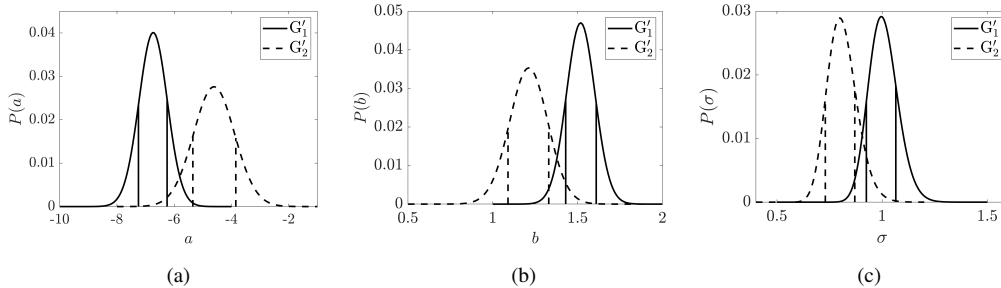


Figure 5: Posterior probability distributions of Amati parameters a , b and σ_{int} for low- z GRBs (group G'_1) and high- z GRBs (group G'_2) with the threshold at $z = 2$. The low- z and high- z distributions are not in agreement and their difference is statistically significant at more than 1σ confidence level for each parameter.

3.1. Main Results

The optimal parameters of the Amati relation are derived through a Bayesian approach, yielding the best-fit values and their associated 1σ uncertainties for the comprehensive dataset G , as summarized in Table 2. Notably, the intercept (a) of the linear Amati relation exhibits a negative value, while its slope demonstrates a positive trend. The intrinsic scatter remains consistently below unity across all instances. Figure 3 visually represents the probability distribution of the three parameters, with vertical lines denoting the 1σ confidence level.

Table 2 also presents the optimal parameters, namely a and b , for the distinct subgroups G_1 and G_2 (with the threshold at $z = 1.5$). The intercept is still negative and the slope is positive in both subgroups. Figure 4 illustrates the probability distributions associated with these subgroups, delineating the distinctive nature of G_1 and G_2 . Vertical lines are employed to mark the 2σ confidence level. Notably, the values of a and b exhibit a discrepancy exceeding the 2σ threshold, indicating a discernible distinction in the GRB populations at low and high redshifts. Despite a smaller value observed at high redshifts, the disparity in the intrinsic scatter is not statistically significant.

Table 3 presents the optimal values of a and b , for the subgroups G'_1 and G'_2 (with the threshold at $z = 2$). Their 1σ errors have also been shown in the respective columns. The continuously negative intercept and positive slope observed in both subgroups underscore a consistent trend. The corresponding posterior probability distributions for these parameters have been shown in Figure 5. The vertical lines have been drawn at 1σ level. The significance is comparatively smaller in this case however, it is still at more than 1σ for both a and b . In this case, the intrinsic scatter is also significantly different for the two subgroups. To illustrate the differences in the $E_{p,i} - E_{iso}$ relations between low- z and high- z GRBs, we present a comparative analysis in Figure 6. The left panel of Figure 6 displays the straight line fits for subgroups G_1 and G_2 , i.e., at the redshift threshold of $z = 1.5$. The solid line represents the fit for low- z GRBs, while the dashed line corresponds to high- z GRBs. The results indicate that the linear fits for low- z and high- z GRBs are distinct, with no overlap between the two groups. Similarly, the right panel presents the straight line fits for the subgroups G'_1 and G'_2 . As in the previous case, both fits are distinct.

To further validate our findings, we computed the AIC for the single linear fit applied across the entire redshift range and the fits for the individual subgroups. The AIC values are presented in Table 4. The AIC for the single linear fit (full z range) is the highest and lowest for subgroups G_1 and G_2 . The double linear fit provides smaller AIC in both cases ($z_{crit} = 1.5$ and 2) than the single linear fit for

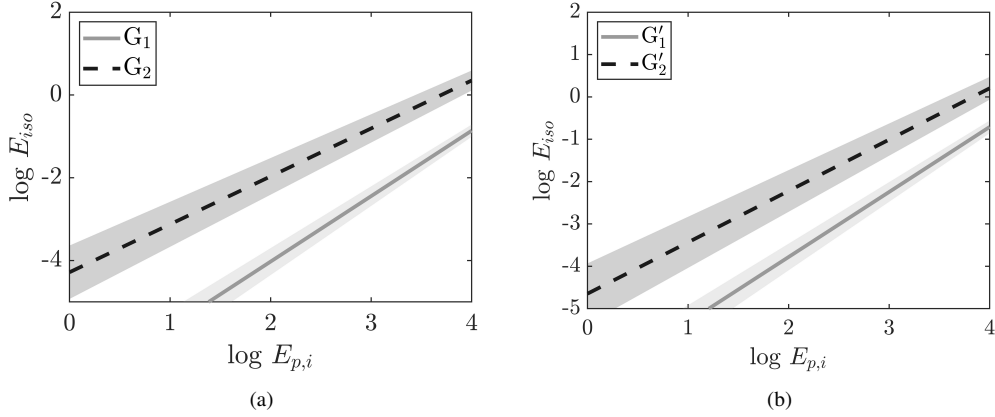


Figure 6: Straight line fit $y = a + bx$ for the subgroups G_1 , G_2 in the left panel and for the subgroups G'_1 , G'_2 in the right panel, where a and b are the best-fit values of Amati parameters.

full data. The difference in AIC values, as defined in Eq. 11, exceeds the threshold for significance. Therefore, the subgroup-based fit at $z_{crit} = 1.5$ is preferred, as it provides a better representation of the data than the single linear fit over the full redshift range.

Table 4: AIC comparison for single linear fit for full redshift range and double linear fits with breaks at $z = 1.5$ and $z = 2$.

Model	z break	AIC
Single Linear Fit (Full Redshift Range)	No	220.98
Double Linear Fit with break at $z = 1.5$	Yes	205.79
Double Linear Fit with break at $z = 2.0$	Yes	212.73

3.2. Probable Instrumental Biases and Selection Effects

Possible biases in each instrument could arise due to their design, calibration, and operational characteristics which may be partly responsible for the observed differences in GRB populations. BAT may exhibit biases related to its coded aperture imaging technique, potentially leading to systematic errors in position determination [49]. It can affect the identification of the host galaxy and hence the redshift measurement. Another issue with the BAT instrument is its capability to detect energies up to 150 keV only [40], which is less than the average peak energy of GRBs [50]. Thus, for several Swift observed GRBs, it is not possible to directly determine the fluence and E_{peak} . FGST's LAT may face biases due to background

noise, energy calibration uncertainties, and instrument response variations across its wide energy range. GBM’s biases could include sensitivity variations across its energy range and potential systematic errors in event classification. While these instruments provide invaluable data, understanding and mitigating biases are crucial for accurate gamma-ray observations.

3.3. *Low- z vs High- z GRB Hosts*

As mentioned in 3.1, we observe significant differences in best-fit values of Amati parameters for low and high- z GRB subgroups. Below we analyse our results in the context of differences in the low- z and high- z GRB host galaxies.

In a detailed study [37] and [51] claim that at high z , long GRBs host galaxies include all morphological types including early-type galaxies. This could be because at high z the early-type galaxies can be observed during their active star formation period. In contrast, star formation in the early-type galaxies at low z is often quenched.

High- z GRB hosts are younger and thus have low metallicities. On the other hand, low- z hosts, especially the early-type ones, are older and have higher metallicities [37]. These differences underscore significant evolutionary changes in galaxy properties and environments from high to low redshifts, affecting the nature and identification of long GRB host galaxies. At a given redshift, dust-obscured GRB hosts are more massive than optically bright galaxies, with massive GRB hosts becoming fairly common at $z > 1.5$ [52]. The authors also link the smaller GRB production at low redshift to metallicity. Using the optically unbiased GRB host (TOUGH) Survey [53] claims that GRB hosts at high z are faint and low in metallicity [54]. The studies based on Damped Lyman α systems at high z support the existence of two GRB progenitor channels, with one being mildly influenced by metallicity [54].

4. Conclusions

This study explored the potential heterogeneity in the Amati correlation among long gamma-ray bursts (GRBs) across varying redshift ranges. Building on earlier investigations by [11, 24, 28, 55], we addressed concerns regarding sample limitations and inconsistencies highlighted by [20] and [39]. By leveraging an expanded dataset of 221 long GRBs, spanning redshifts from 0.034 to 8.2, we conducted a comprehensive analysis to better understand the redshift dependence of the Amati relation. Our findings reveal statistically significant variations in the Amati relation parameters across different redshift subgroups. When dividing the dataset at

critical redshifts, $z_{\text{crit}} = 1.5$ and $z_{\text{crit}} = 2.0$, the fitting parameters a and b showed noticeable differences. At $z_{\text{crit}} = 2$, the low- and high-redshift subgroups exhibited a difference of more than 1σ . At $z_{\text{crit}} = 1.5$, the differences exceeded 2σ for a and b parameters, indicating a more pronounced distinction between low- and high-redshift GRB populations. These variations may be attributed to intrinsic factors such as host galaxy metallicity, although selection effects or instrumental biases could also play a role. Our findings align with those of [28], who reported similar discrepancies at $z_{\text{crit}} = 1.5$ using a different dataset. Furthermore, the Akaike Information Criterion (AIC) analysis favored a double-line fit with a break at $z = 1.5$ over a single-line fit, reinforcing the idea that GRBs may exhibit distinct properties across redshift ranges. Looking ahead, upcoming missions such as the *Transient High-Energy Sky and Early Universe Surveyor* (THESEUS), slated for launch in 2032 [56], and the *enhanced X-ray Timing and Polarimetry* (eXTP) mission [57], promise to advance our understanding of high-redshift GRBs. THESEUS aims to detect GRBs up to $z = 12$, while eXTP is expected to observe approximately 100 GRBs annually, offering enhanced sensitivity and broader observational coverage. These missions will provide the precision and data volume necessary to validate our results and further clarify the differences between low- and high-redshift GRB populations.

Acknowledgments

Meghendra Singh thanks DMRC for support. Darshan Singh thanks the co-peers of GD Goenka University for eternal assistance.

References

- [1] D. Band, J. Matteson, L. Ford, B. Schaefer, et al., Batse observations of gamma-ray burst spectra. i. spectral diversity, *The Astrophysical Journal* 413 (1993) 281.
- [2] P. Kumar, B. Zhang, The physics of gamma-ray bursts and relativistic jets, *Physics Reports* 561 (2014) 1–109.
- [3] C. Kouveliotou, C. A. Meegan, G. J. Fishman, N. P. Bhat, et al., Identification of two classes of gamma-ray bursts, *Astrophysical Journal Letters* 413 (1993) L101.
- [4] L. Amati, To be short or long is not the question, *Nature Astronomy* 5 (2021) 877–878.

- [5] L. Amati, F. Frontera, M. Tavani, J. J. M. in 't Zand, et al., Intrinsic spectra and energetics of beposax gamma-ray bursts with known redshifts, Monthly Notices of the Royal Astronomical Society 390 (2002) 81–89.
- [6] L. Amati, The $E_{p,i} - E_{iso}$ correlation in gamma-ray bursts: updated observational status, re-analysis and main implications, Monthly Notices of the Royal Astronomical Society 372 (2006) 233–245.
- [7] L. Amati, C. Guidorzi, F. Frontera, M. D. Valle, et al., Measuring the cosmological parameters with the $E_{p,i} - E_{iso}$ correlation of gamma-ray bursts, Monthly Notices of the Royal Astronomical Society 391 (2008) 577–581.
- [8] L. Amati, F. Frontera, C. Guidorzi, Extremely energetic fermi gamma-ray bursts obey spectral energy correlations, Astronomy & Astrophysics 508 (2009) 173–180.
- [9] D. Yonetoku, T. Murakami, T. Nakamura, R. Yamazaki, et al., Gamma-ray burst formation rate inferred from the spectral peak energy–peak luminosity relation, The Astrophysical Journal 609 (2009) 635.
- [10] G. Ghirlanda, G. Ghisellini, D. Lazzati, C. Firmani, Gamma ray bursts: New rulers to measure the universe, The Astrophysical Journal 613 (2004) L13–L16.
- [11] G. Ghirlanda, L. Nava, G. Ghisellini, Spectral-luminosity relation within individual fermi gamma rays bursts, Astronomy & Astrophysics 511 (2010) A43.
- [12] M. G. Dainotti, V. Nielson, G. Sarracino, E. Rinaldi, et al., Optical and x-ray grb fundamental planes as cosmological distance indicators, Monthly Notices of the Royal Astronomical Society 514 (2022) 1828–1856.
- [13] F. Daigne, E. M. Rossi, R. Mochkovitch, The redshift distribution of swift gamma-ray bursts: evidence for evolution, Monthly Notices of the Royal Astronomical Society 372 (2006) 1034–1042.
- [14] R. Basak, A. R. Rao, Pulse-wise amati correlation in fermi gamma-ray bursts, Monthly Notices of the Royal Astronomical Society: Letters 436 (2013) 3082–3088.

- [15] Y. Dai, X.-G. Zheng, Z.-X. Li, H. G. et al., Redshift evolution of the amati relation: Calibrated results from the hubble diagram of quasars at high redshifts, *Astronomy & Astrophysics* 651 (2021) L8.
- [16] L. Huang, Z. Huang, X. Luo, X. He, et al., Reconciling low and high redshift grb luminosity correlations, *Physical Review D* 103 (2021) 123521.
- [17] H.-N. Lin, X. Li, Z. Chang, Model-independent distance calibration of high-redshift gamma-ray bursts and constrain on the λ cdm model, *Monthly Notices of the Royal Astronomical Society* 455 (2) (2016) 2131–2138.
- [18] M. Demianski, E. Piedipalumbo, D. Sawant, L. Amati, Cosmology with gamma-ray bursts: I. the hubble diagram through the calibrated E_p, i – E_{iso} correlation, *Astronomy & Astrophysics* 598 (2017) A112.
- [19] S. Cao, N. Khadka, B. Ratra, Standardizing dainotti-correlated gamma-ray bursts, and using them with standardized amati-correlated gamma-ray bursts to constrain cosmological model parameters, *Monthly Notices of the Royal Astronomical Society* 510 (2021) 2928–2947.
- [20] N. Khadka, O. Luongo, M. Muccino, B. Ratra, Do gamma-ray burst measurements provide a useful test of cosmological models, *Journal of Cosmology and Astroparticle Physics* (2021) 42.
- [21] X. D. Jia, J. P. Hu, J. Yang, B. B. Zhang, et al., The E_p, i – E_{iso} correlation of gamma-ray bursts: calibration and cosmological applications, *Monthly Notices of the Royal Astronomical Society* 516 (2022) 2575–2585.
- [22] E. Ó. Colgáin, M. M. Sheikh-Jabbari, L. Yin, Do high redshift QSOs and GRBs corroborate JWST?, 10.48550/arXiv.2405.19953 (May 2024).
- [23] M. G. Dainotti, V. F. Cardone, E. Piedipalumbo, S. Capozziello, Slope evolution of grb correlations and cosmology, *Monthly Notices of the Royal Astronomical Society* 436 (2013) 82–88.
- [24] Li-Xin Li, Variation of the amati relation with cosmological redshift: a selection effect or an evolution effect?, *Monthly Notices of the Royal Astronomical Society: Letters* 379 (2007) L55–L59.
- [25] J. J. Geng, Y. F. Huang, On the correlation of low-energy spectral indices and redshifts of gamma-ray bursts, *The Astrophysical Journal* 764 (2013) 75.

- [26] R. Tsutsui, D. Yonetoku, T. Nakamura, K. Takahashi, et al., Possible existence of the $E_p - L_p$ and $E_{p,i} - E_{iso}$ correlations for short gamma-ray bursts with a factor 5–100 dimmer than those for long gamma-ray bursts, *Monthly Notices of the Royal Astronomical Society* 431 (2013) 1398–1404.
- [27] H.-N. Lin, X. Li, S. Wang, Z. Chang, Are long gamma-ray bursts standard candles?, *Monthly Notices of the Royal Astronomical Society* 453 (1) (2015) 128–132.
- [28] M. Singh, D. Singh, D. Verma, et al., Investigating the evolution of amati parameters with redshift, *Research in Astronomy and Astrophysics* 24 (2024) 015015.
- [29] D. Kumar, N. Rani, D. Jain, S. Mahajan, A. Mukherjee, Gamma rays bursts: a viable cosmological probe?, *Journal of Cosmology and Astroparticle Physics* 2023 (07) (2023) 021.
- [30] N. R. Butler, D. Kocevski, J. S. Bloom, Generalized tests for selection effects in gamma-ray burst high-energy correlations, *The Astrophysical Journal* 694 (2009) 76–83.
- [31] H. Zitouni, N. Guessoum, W. J. Azzam, Revisiting the amati and yonetoku correlations with swift grbs, *Astrophysics and Space Science* 351 (2014) 267–280.
- [32] A. Mortlock, C. J. Conselice, W. G. Hartley, J. R. Owers, C. Lani, A. F. Bluck, O. Almaini, K. Duncan, A. v. d. Wel, A. M. Koekemoer, et al., The redshift and mass dependence on the formation of the hubble sequence at $z < 1$ from candels/uds, *Monthly Notices of the Royal Astronomical Society* 433 (2) (2013) 1185–1201.
- [33] A. Mortlock, C. J. Conselice, W. G. Hartley, J. R. Owers, et al., The redshift and mass dependence on the formation of the hubble sequence at $z > 1$ from candels/uds, *Monthly Notices of the Royal Astronomical Society* 434 (2013) 1185–1201.
- [34] C. J. Conselice, The evolution of galaxy structure over cosmic time, *Astronomy and Astrophysics* 52 (2014) 291–337.

- [35] L. Ferreira, C. J. Conselice, E. Sazonova, F. Ferrari, et al., The jwst hubble sequence: The rest-frame optical evolution of galaxy structure at $1.5 < z < 8$, *The Astrophysical Journal* 938 (2022) L2.
- [36] F. Y. Wang, Z. G. Dai, Long grbs are metallicity-biased tracers of star formation: evidence from host galaxies and redshift distribution, *The American Astronomical Society* 213 (2014) 15.
- [37] M. Palla, F. Matteucci, F. Calura, F. Longo, Galactic archaeology at high redshift: Inferring the nature of grb host galaxies from abundances, *The Astrophysical Journal* 889 (2020) 4.
- [38] I. Labbé, P. van Dokkum, E. Nelson, R. Bezanson, K. A. Suess, J. Leja, G. Brammer, K. Whitaker, E. Mathews, M. Stefanon, B. Wang, A population of red candidate massive galaxies 600 Myr after the Big Bang, *Nature* 616 (7956) (2023) 266–269.
- [39] F. F. Dirirsa, S. Razzaque, F. Piron, M. Arimoto, M. Axelsson, D. Kocevski, F. Longo, M. Ohno, S. Zhu, Spectral analysis of fermi-lat gamma-ray bursts with known redshift and their potential use as cosmological standard candles, *The Astrophysical Journal* 887 (1) (2019) 13.
- [40] N. Gehrels, G. Chincarini, P. Giommi, K. O. Mason, et al., The swift gamma-ray burst mission, *The Astrophysical Journal* 611 (2011) 1005.
- [41] W. B. Atwood, A. A. Abdo, M. Ackermann, W. A. et al., The large area telescope on the fermi gamma-ray space telescope mission, *The Astrophysical Journal* 697 (2009) 1071.
- [42] D. E. Reichart, D. Q. Lamb, E. E. Fenimore, E. Ramirez-Ruiz, et al., A possible cepheid-like luminosity estimator for the long gamma-ray bursts, *The Astrophysical Journal* 552 (2001) 57–71.
- [43] D. A. Perley, T. Krühler, S. Schulze, A. de Ugarte Postigo et al., The swift gamma-ray burst host galaxy legacy survey - i. sample selection and redshift distribution, *The Astrophysical Journal* 817 (2016) 7.
- [44] L. G. Balazs, A. Meszaros, I. Horvath, Anisotropy of the sky distribution of gamma-ray bursts, *Astronomy & Astrophysics* 339 (1998) 1–6.

- [45] U. Andrade, C. A. P. Bengaly, J. S. Alcaniz, S. Capozziello, Revisiting the statistical isotropy of grb sky distribution, *Monthly Notices of the Royal Astronomical Society* 490 (2019) 4481–4488.
- [46] S. K. Sethi, S. G. Bhargavi, J. Greiner, On the clustering of grbs on the sky, *AIP Conference Proceedings* 526 (2000) 107.
- [47] H. Akaike, A new look at the statistical model identification, *IEEE transactions on automatic control* 19 (6) (1974) 716–723.
- [48] H. Akaike, Factor analysis and aic, *Psychometrika* 52 (1987) 317–332.
- [49] S. D. Barthelmy, L. M. Barbier, J. R. Cummings, E. E. Fenimore, et al., The burst alert telescope (bat) on the swift midex mission, *Space Science Reviews* 120 (2005) 143–164.
- [50] Y. Kaneko, R. D. Preece, M. S. Briggs, W. S. Paciesas, et al., The complete spectral catalog of bright batse gamma-ray bursts, *Astrophysical Journal Supplement Series* 166 (2006) 298–340.
- [51] V. Grieco, F. Matteucci, F. Calura, S. Boissier, et al., Chemical evolution models: Grb host identification and cosmic dust predictions, *Monthly Notices of the Royal Astronomical Society* 444 (2014) 1054–1065.
- [52] D. A. Perley, A. J. Levan, N. R. Tanvir, S. B. C. et al., A population of massive, luminous galaxies hosting heavily dust-obscured gamma-ray bursts: implications for the use of grbs as tracers of cosmic star formation, *The Astrophysical Journal* 778 (2013) 128.
- [53] S. Schulze, R. Chapman, J. Hjorth, A. J. Levan, et al., The optically unbiased grb host (tough) survey. vii. the host galaxy luminosity function: probing the relationship between grbs and star formation to redshift 6, *The Astrophysical Journal* 808 (2015) 73.
- [54] A. Cucchiara, M. Fumagalli, M. Rafelski, D. Kocevski, et al., Unveiling the secrets of metallicity and massive star formation using dlas along gamma-ray bursts, *Astrophysical Journal* 804 (2015) 16.
- [55] G. J. Wang, H. Yu, Zheng-Xiang, J.-Q. X. et al., Evolutions and calibrations of long gamma-ray-burst luminosity correlations revisited, *The Astrophysical Journal* 836 (2017) 103.

- [56] G. Ghirlanda, R. Salvaterra, M. Toffano, S. Ronchini, et al., Gamma ray burst studies with theseus, *Experimental Astronomy* 52 (2021) 277–308.
- [57] S. N. Zhang, A. S. M. F. Y. X. et al., The enhanced x-ray timing and polarimetry mission—extp, *Science China Physics, Mechanics, and Astronomy* 62 (2019) 29502.